metals

MDPI

Article

A New Cumulative Fatigue Damage Rule Based on Dynamic Residual S-N Curve and Material Memory Concept

Zhaochun Peng [1,2], Hong-Zhong Huang [1,2,*], Jie Zhou [1,2] and Yan-Feng Li [1,2]

[1] School of Mechanical and Electrical Engineering, University of Electronic Science and Technology of China, Chengdu 611731, China; zcpeng2012@163.com (Z.P.); zhoujseven@gmail.com (J.Z.); Yanfengli@uestc.edu.cn (Y.-F.L.);

[2] Center for System Reliability and Safety, University of Electronic Science and Technology of China, Chengdu 611731, China

* Correspondence: hzhuang@uestc.edu.cn; Tel.: +86-28-6183-1252

Received: 23 May 2018; Accepted: 7 June 2018; Published: 14 June 2018

Abstract: This paper introduces a new phenomenological cumulative damage rule to predict damage and fatigue life under variable amplitude loading. The rule combines a residual S-N curve approach and a material memory concept to describe the damage accumulation behavior. The residual S-N curve slope is regarded as a variable with respect to the loading history. The change in slope is then used as a damage measure and quantified by a material memory degeneration parameter. This model improves the traditional linear damage rule by taking the load-level dependence and loading sequence effect into account, which still preserves its superiority. A series of non-uniform fatigue loading protocols are used to demonstrate the effectiveness of the proposed model. The prediction results using the proposed model are more accurate than those using three popular damage models. Moreover, several common characteristics and fundamental properties of the chosen fatigue models are extracted and discussed.

Keywords: fatigue; cumulative damage; residual S-N curve; material memory; life prediction

1. Introduction

In practical engineering, most structural components and mechanical parts in service usually endure the cyclic fluctuating loads with varying intensity. Fatigue is the major cause of the catastrophic failures of these elements or parts. Fatigue failure invariably occurs in the localized weak areas of the material and permanently deteriorates its performance and safe usage. The concept of damage is typically assigned to characterize such a failure process and also plays a fundamental role in fatigue life prediction [1–5]. In spite of extensive investigations to address fatigue theories, the problem of assessing the extent of fatigue damage and then predicting fatigue life still remains a major challenge in fatigue resistant design. Therefore, a reliable cumulative damage rule is strongly expected in structural integrity, reliability-based design, and safety assessments [6]. It should contribute to the increased prediction accuracy, and especially, to obtain maintenance strategies for replacing the damaged elements or parts before failure.

Essentially, fatigue damage mainly includes the process of crack initiation and crack propagation involving various micro-scale behaviors, such as surface extrusion-intrusion, dislocations, plastic slip bands, vacancies, and crack coalescence [7,8]. Although great advancements have been made in the micro-physical mechanisms of fatigue failure, it is not surprising that such analytical theories are relatively complicated and difficult to implement in engineering. In contrast, phenomenological theories [9–14] are still the main approaches for fatigue analysis, where simple fatigue formulas

that can be identified directly from experiments are preferred. In cases of uniform fatigue loading, some phenomenological formulas are representative and constitute the generic fatigue rules available for many different materials, such as Basquin's law (stress-life), Manson-Coffin's law (strain-life), Goodman's law (mean stress correction), and Paris' law (crack propagation rate).

However, the fatigue modeling under non-uniform cyclic loading becomes much more intractable due to the complexity of loading histories. In such a fatigue loading, assessment of the damage and fatigue life often relies on cumulative damage theories, including various linear and non-linear hypotheses. A comprehensive overview of cumulative damage and life predictive models has been achieved by Fatemi and Yang [15] and Schijve [16]. The Palmgren-Miner's hypothesis [17] is acknowledged as a pioneering research on the linear damage rule (LDR) as well as a unified methodology to address fatigue issues under arbitrary non-uniform loading protocols, in spite of limited physical insights and non-conservative predictions. Many researchers suggested that the prediction error of LDR is not necessarily responsible for the linear summation form but mainly responsible for the lack of load-level dependence and loading sequence effects [15,18,19]. Despite the major deficiencies, LDR is still dominantly used in practical engineering design, because the linear summation form can significantly reduce the calculation effort. In order to improve the LDR, a considerable number of non-linear hypotheses [20–24] are proposed to explain the loading sequence observed in the experiments, yet most of them substantially need more parameters to calibrate and are often computationally expensive, especially for multi-stage block loadings when compared with the LDR. The main advantages of LDR lie in its conceptual simplicity, in following a simple linear summation of damage that is inexpensive both computationally and experimentally, and particularly in a small amount of data necessary from the Basquin's law (S-N curve).

In recent years, fatigue damage modeling in terms of the S-N curve approach has been reported quite intensively and received increasing attention in fatigue life prediction. Corten and Dolan [25] and Freudenthal and Heller [26] put forward a clockwise rotation method of the S-N curve to account for the load interaction effects. Subramanyan [27] introduced an isodamage line to present the damage accumulation process and all of the damage lines were assumed to converge into the knee point of the S-N curve around the endurance limit. Hashin and Rotem [28] extended Subramanyan's hypothesis and presented a discussion of damage curve families that could pass through either static ultimate or endurance point. Leipholz [29] demonstrated an analytical life-reducing approach to obtain a modified S-N curve, which intersects the original curve at a higher stress level and deviates from it at lower ones. Liu and Mahadevan [19] developed a non-linear cumulative damage model based on the LDR theory, together with a stochastic S-N curve technique, to predict the probabilistic fatigue life of metallic materials under both constant and variable loadings. Lately, Aghoury and Galal [30] proposed a stress-life damage accumulation model by using a concept of virtual target life curve (VTLC) derived from the conventional S-N curve. In this model, fatigue damage is defined as the accumulated loss of the expected life in VTLC, and the loading amplitudes and overloading effects can be captured. Kwofie and Rahbar [31] pointed out that the fatigue failure process was probably dominated by the fatigue driving stress in materials, while also formulating a simple cumulative damage rule using the regular S-N curve. Peng et al. [32] subsequently improved the theory with the strain energy parameter, resulting in more accurate calculations. Several researchers [33–37] suggested a new framework for the damaged stress models connected to the S-N curve to address various fatigue programs, including variable, random, uniaxial, and multiaxial loadings. As stated above, the basic idea of these modeling approaches is to alleviate the effects caused by shortcomings of LDR by considering additional damaging effects responsible for the loading histories. However, most of them are based on the non-linear damage theories, which may cause a large amount of calculation [38,39]. The cumulative damage models are mainly derived from the transformation of the conventional S-N curve that is only suitable for the virgin material without initial damage. Moreover, from the phenomenological point of view, the fatigue damage accumulation is a direct result of irreversible

degradation of material properties, whereas the existing models fail to characterize the degradation mechanisms on damage accumulation.

In this paper, a phenomenological damage accumulation model for predicting damage and fatigue life under variable amplitude loading is proposed, which incorporates a residual S-N curve approach and a material memory concept [40]. The residual S-N curve is used to describe the stress-life relation of the damaged material and its slope is considered as a variable with respect to the loading history. Fatigue damage is measured by assessing the change in slope or slope ratio. Then, the material memory concept is introduced to present the material degradation behavior and quantify the slope ratio when accumulating fatigue damage. The proposed model aims to improve the performance of the LDR to make it load-level dependent while still preserving the superiority. A series of experimental data in the literature are used to verify the effectiveness of the model, which covers several metallic materials under non-uniform fatigue loading protocols (two-stage and multi-stage). Moreover, three commonly used cumulative damage rules are chosen for the model comparisons.

2. Formulation of the Proposed Model and Commonly Used Cumulative Damage Rules

2.1. Proposed Model

The usual way of analyzing and predicting fatigue life of metallic materials or components is to plot the stress amplitude against the number of loading cycles to failure, i.e., S-N diagram. It is widely accepted that the basic stress-life relation can be expressed by the Basquin's power law [41], shown as:

$$\sigma^m N_f = C \text{ or } \sigma = \sigma'_f \left(2N_f\right)^h \tag{1}$$

where N_f is the number of loading cycles to failure at a given stress level σ; m and C are material constants; σ'_f and h denote the fatigue strength coefficient and fatigue strength exponent, respectively. Equation (1) can be rewritten as a linear function in log-log coordinates, as shown in Figure 1, that is:

$$\log(\sigma) = a + b\log(N_f) \tag{2}$$

where a is the intercept and b is the slope ($b = -1/m$).

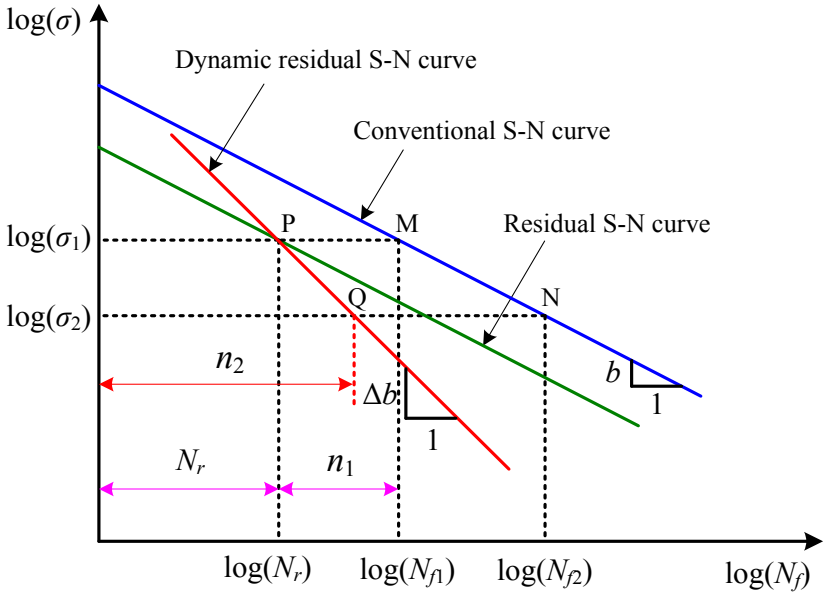

Figure 1. Schematic representation of conventional S-N curve, residual S-N curve, and dynamic residual S-N curve.

Given that a specimen suffers the initial damage induced by the loading stress amplitude σ_1 for n_1 cycles, the residual number of cycles to fracture (residual life N_r) at the same stress amplitude is $N_r = N_{f1} - n_1$ (see Figure 1). For the undamaged specimen, the residual life corresponds to the fatigue failure cycles determined from the conventional S-N curve. Considering the damaged specimen as an undamaged one, a simple procedure for describing the stress-life relation of the damaged specimen is to use the residual S-N curve, which is assumed to have a similar mathematical description of the conventional one. Thus, a residual S-N curve with the same slope in Equation (2) can take the form:

$$\log(\sigma) = a' + b\log(N_r) \tag{3}$$

where a' is the intercept of residual S-N curve.

For variable amplitude loading tests, particular attention is often given to the commonly used and simplest case of the two-stage cyclic loading. Under laboratory loading condition, such loading pattern is defined as the procedure that the specimen is first pre-cycled at a certain stress amplitude σ_1 for n_1 cycles, then cycled at another stress amplitude σ_2 for n_2 cycles to failure. The relationship between Equations (2) and (3) means to a linear cumulative damage rule, that is:

$$\frac{n_1}{N_{f1}} + \frac{n_2}{N_{f2}} = 1 \tag{4}$$

According to this, Equation (3) is thus called the Miner's residual S-N curve, because the slope in Equation (3) is the same as that in Equation (2). Since Equation (4) does not consider the effect of loading histories, the slope in Equation (3) may be a dominant factor of describing the loading effects on fatigue. In this work, the residual S-N curve slope is considered as a variable with respect to the previous fatigue loadings, instead of a basic material constant. Then, a dynamic residual S-N curve, as shown in Figure 1, can be expressed as:

$$\log(\sigma) = a'' + \Delta b\log(N_r) \tag{5}$$

where a'' is the intercept and Δb is the dynamic slope.

The fatigue behaviors responsible for Equation (5) can be described as: for the material in virgin state without initial damage, Δb is identical to the original slope b; as the fatigue loading continues, the absolute value of Δb increases with the progressive fatigue damage; at fracture, it tends to be infinite. Consequently, the slope ratio $b/\Delta b$, which is defined as b_r for later convenience, will decrease with the loading cycles or the expended life fraction and should range from 1 to 0. In the dynamic residual S-N curve method, the change in slope is appropriate to present the fatigue failure process and the evolution law of damage accumulation. It is essential to quantify b_r when accumulating fatigue damage.

Recently, Böhm et al. [40,42] presented a material memory concept that was taken from the psychology domain for fatigue damage analysis. There are some similarities between the human memory and the material properties. In general, the human memory performance is described as an exponential function of time, for example the Ebbinghaus forgetting curve [43]. Through taking the fatigue loading cycles to replace the time function, their authors also suggested a material memory function as:

$$M = (A - B)e^{-\frac{n}{d}} + B \tag{6}$$

where M is the material memory performance; A is the memorization factor; B is the asymptote; d denotes the reverse of forgetting factor that is given by fatigue cycles and recommended as $d = N_f$ for simplicity. The forgetting curve is shown in Figure 2.

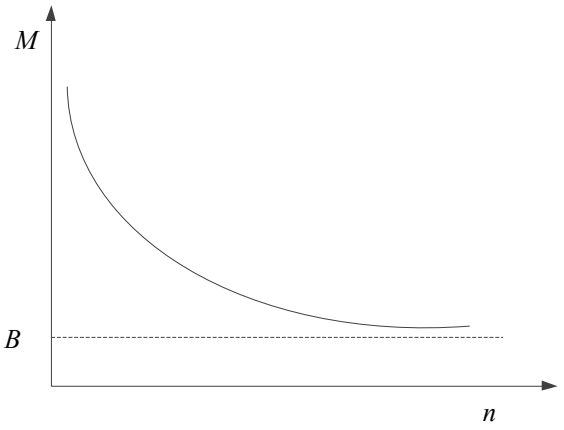

Figure 2. The forgetting curve.

From Equation (6), the performance measure of material memory degenerates progressively under the cyclic loading. At the initial state, i.e., n = 0, the memory performance is $M|_{n=0} = A$; when the material is fatigued, it will decrease with the accumulated loading cycles, and $M|_{n=N_f} = (A-B)e^{-1} + B$; at the critical state, i.e., $n = N_f$,$M|_{n=N_f} = (A-B)e^{-1} + B$. In order to present the degree of degradation, a decay coefficient of the material memory performance is introduced and simply described as follows:

$$\alpha = \frac{M|_n - M|_{n=N_f}}{M|_{n=0} - M|_{n=N_f}} = \frac{\left[(A-B)e^{-n/N_f} + B\right] - \left[(A-B)e^{-1} + B\right]}{A - \left[(A-B)e^{-1} + B\right]} = \frac{e^{-\frac{n}{N_f}} - e^{-1}}{1 - e^{-1}} \tag{7}$$

It is noted that α is a function of the expended life fraction and varies from 1 to 0. For the initial condition, i.e., $n/N_f = 0$, $\alpha = 1$, the material is undamaged without degeneration; after that, α decreases with the fatigue loading cycles; when $n/N_f = 1$, $\alpha = 0$, the material will fully be degenerated. To a certain extent, this decay coefficient can correctly characterize the fatigue damage behaviors and the damaged degree of the material. As stated before, the slope ratio b_r in dynamic residual S-N curve is used to characterize the evolution law of damage accumulation. Thus, it is suitable to use the degeneration parameter of α to quantify b_r.

In the case of two-stage cyclic loading, the material is fatigued by the first stress amplitude σ_1 for n_1 cycles, and the slope in Equation (5) becomes Δb_1. The change in slope from b to Δb_1 represents the damage degree of the material, which can be characterized by the decay coefficient α. Besides, α satisfies the boundary conditions (it ranges from 1 to 0) with respect to $b/\Delta b_1$. Therefore, the slope ratio for the first operation can be assumed as:

$$b_{r1} = \frac{b}{\Delta b_1} = \alpha_1 = \frac{e^{-\frac{n_1}{N_{f1}}} - e^{-1}}{1 - e^{-1}} \tag{8}$$

According to the conventional S-N curve in Figure 1, the points M (N_{f1}, σ_1) and N (N_{f2}, σ_2) should satisfy Equation (2), that is:

$$\log(\sigma_1) = a + b\log(N_{f1}) \tag{9}$$

$$\log(\sigma_2) = a + b\log(N_{f2}) \tag{10}$$

Subtracting Equation (10) from Equation (9) gives:

$$\log\left(\frac{\sigma_1}{\sigma_2}\right) = b\log\left(\frac{N_{f1}}{N_{f2}}\right) \tag{11}$$

In the dynamic residual S-N curve, the residual life at the second stress amplitude σ_2 is $N_{r2} = n_2$, and the points P ($N_{f1} - n_1$, σ_1) and Q (n_2, σ_2) should satisfy Equation (5), that is:

$$\log(\sigma_1) = a'' + \Delta b_1 \log(N_{f1} - n_1) \tag{12}$$

$$\log(\sigma_2) = a'' + \Delta b_1 \log(n_2) \tag{13}$$

Subtracting Equation (13) from Equation (12), we obtain:

$$\log\left(\frac{\sigma_1}{\sigma_2}\right) = \Delta b_1 \log\left(\frac{N_{f1} - n_1}{n_2}\right) \tag{14}$$

Combing Equations (11) and (14) yields:

$$\frac{b}{\Delta b_1} \log\left(\frac{N_{f1}}{N_{f2}}\right) = \log\left(\frac{N_{f1} - n_1}{n_2}\right) = \log\left(\frac{N_{f1}}{N_{f2}} \times \frac{1 - \frac{n_1}{N_{f1}}}{\frac{n_2}{N_{f2}}}\right) \tag{15}$$

Substituting Equation (8) into Equation (15), the life fraction at the second loading level can be derived as:

$$\frac{n_2}{N_{f2}} = \left(1 - \frac{n_1}{N_{f1}}\right)\left(\frac{N_{f1}}{N_{f2}}\right)^{1-\alpha_1} = \left(1 - \frac{n_1}{N_{f1}}\right)\left(\frac{N_{f1}}{N_{f2}}\right)^{\frac{1-e^{-n_1/N_{f1}}}{1-e^{-1}}} \tag{16}$$

For the high-low loading sequence ($0 < N_{f1}/N_{f2} < 1$), the sum of the expended life fractions is:

$$\sum_{i=1}^{2} \frac{n_i}{N_{fi}} = \frac{n_1}{N_{f1}} + \left(1 - \frac{n_1}{N_{f1}}\right)\left(\frac{N_{f1}}{N_{f2}}\right)^{1-\alpha_1} < 1 \tag{17}$$

For the low-high loading sequence ($N_{f1}/N_{f2} > 1$), it is:

$$\sum_{i=1}^{2} \frac{n_i}{N_{fi}} = \frac{n_1}{N_{f1}} + \left(1 - \frac{n_1}{N_{f1}}\right)\left(\frac{N_{f1}}{N_{f2}}\right)^{1-\alpha_1} > 1 \tag{18}$$

Considering that the final fracture occurs when the cumulative damage reaches a failure threshold of $D_f = 1$, by rearranging Equation (16), one can obtain a failure criterion of cumulative damage as follows:

$$\frac{n_1}{N_{f1}} + \frac{n_2}{N_{f2}}\left(\frac{N_{f1}}{N_{f2}}\right)^{\alpha_1 - 1} = 1 \tag{19}$$

For a three-stage fatigue loading, using a similar analytical method and derivation procedure of the two-stage loading, the slope ratio and the life fraction at the third loading level can be expressed by Equations (20) and (21), respectively:

$$b_{r2} = \frac{b}{\Delta b_2} = \frac{b}{\Delta b_1} \times \frac{\Delta b_1}{\Delta b_2} = \alpha_1 \times \alpha_2 = \frac{e^{-\frac{n_1}{N_{f1}}} - e^{-1}}{1 - e^{-1}} \times \frac{e^{-\frac{n_2}{N_{f2}}} - e^{-1}}{1 - e^{-1}} \tag{20}$$

$$\frac{n_3}{N_{f3}} = \left(\left(1 - \frac{n_1}{N_{f1}}\right)\left(\frac{N_{f1}}{N_{f2}}\right)^{1-\alpha_1} - \frac{n_2}{N_{f2}}\right)\left(\frac{N_{f2}}{N_{f3}}\right)^{1-\alpha_1\alpha_2} \tag{21}$$

By rearranging Equation (21), it leads to the following failure criterion:

$$\frac{n_1}{N_{f1}} + \frac{n_2}{N_{f2}}\left(\frac{N_{f1}}{N_{f2}}\right)^{\alpha_1 - 1} + \frac{n_3}{N_{f3}}\left(\frac{N_{f2}}{N_{f3}}\right)^{\alpha_1\alpha_2 - 1}\left(\frac{N_{f1}}{N_{f2}}\right)^{\alpha_1 - 1} = 1 \tag{22}$$

It should be pointed out that Equations (20) and (22) can be generalized to the multi-stage loading protocols. The representation of the slope ratio for the *i*-level fatigue loading is calculated by:

$$b_{r(i-1)} = \frac{b}{\Delta b_{i-1}} = \frac{b}{\Delta b_1} \times \frac{\Delta b_1}{\Delta b_2} \times \cdots \times \frac{\Delta b_{i-2}}{\Delta b_{i-1}} = \alpha_1 \times \alpha_2 \times \cdots \times \alpha_{i-1} = \prod_1^{i-1} \frac{e^{-\frac{n_i}{N_{fi}}} - e^{-1}}{1 - e^{-1}} \tag{23}$$

Accordingly, the cumulative damage criterion of fatigue failure can be derived as:

$$\frac{n_1}{N_{f1}} + \frac{n_2}{N_{f2}}\left(\frac{N_{f1}}{N_{f2}}\right)^{\alpha_1 - 1} + \frac{n_3}{N_{f3}}\left(\frac{N_{f2}}{N_{f3}}\right)^{\alpha_1\alpha_2 - 1}\left(\frac{N_{f1}}{N_{f2}}\right)^{\alpha_1 - 1} + \frac{n_4}{N_{f4}}\left(\frac{N_{f3}}{N_{f4}}\right)^{\alpha_1\alpha_2\alpha_3 - 1}\left(\frac{N_{f2}}{N_{f3}}\right)^{\alpha_1\alpha_2 - 1}\left(\frac{N_{f1}}{N_{f2}}\right)^{\alpha_1 - 1} + \cdots = 1 \tag{24}$$

For each item in Equation (24), a general form of the damage variable D_i is obtained as:

$$D_i = \frac{n_i}{N_{fi}} \times \prod_{j=1}^{i-1}\left(\frac{N_{fj}}{N_{f(j+1)}}\right)^{(\prod_{k=1}^{j} \frac{e^{-\frac{n_k}{N_{fk}}} - e^{-1}}{1 - e^{-1}}) - 1} \tag{25}$$

Therefore, a new cumulative fatigue damage rule yields:

$$\sum D_i = \sum_1^i \frac{n_i}{N_{fi}} \times \prod_{j=1}^{i-1}\left(\frac{N_{fj}}{N_{f(j+1)}}\right)^{(\prod_{k=1}^{j} \frac{e^{-\frac{n_k}{N_{fk}}} - e^{-1}}{1 - e^{-1}}) - 1} = 1 \tag{26}$$

Note that Equation (25) relates to the parameters of expended life fraction and fatigue failure lives, and they can be determined directly from the experimental data and conventional S-N curve. In Equation (24), fatigue damage is accumulated by taking a linear summation of the segmental damage caused by each loading stress level. For constant amplitude loading, $N_{f1} = N_{f2} = \ldots = N_{fi}$ and that $N_{fj}/N_{f(j+1)} = 1$, then Equation (26) degenerates to the Miner rule. Hence, Miner rule can be viewed as a particular case of the proposed model under constant amplitude loading. As a matter of fact, the proposed model improves the Miner rule by multiplying a load effect coefficient in connection with previous fatigue loadings to represent the loading sequence effect.

2.2. Typical Cumulative Damage Rules

In this study, three typical and commonly used cumulative damage rules, i.e., Palmgren-Miner rule, Corten-Dolan rule, and Kwofie-Rahbar rule, are chosen and briefly reviewed for analysis.

2.2.1. Palmgren-Miner Rule (Miner Rule for Short)

The initial treatment of cumulative fatigue damage is the LDR, i.e., Palmgren-Miner rule or Miner rule [17], with a basic assumption of constant work absorption in materials. In this rule, fatigue damage accumulates progressively in a linear manner, and the cumulative damage at failure is assumed as $D_f = 1$. Mathematically, Miner rule can be expressed as:

$$\sum D_i = \frac{n_1}{N_{f1}} + \frac{n_2}{N_{f2}} + \frac{n_3}{N_{f3}} + \frac{n_4}{N_{f4}} + \cdots = 1 \tag{27}$$

The damage variable for each loading stress level is given by:

$$D_i = \frac{n_i}{N_{fi}} \tag{28}$$

In Equation (28), the measure of fatigue damage is simply defined as a life fraction or cycle ratio. The load effect coefficient can be taken as unity without considering fatigue loading histories.

2.2.2. Corten-Dolan Rule (Corten's Model for Short)

Corten-Dolan rule [25] is one of the earliest theories to predict load interaction effects by modifying the slope of conventional S-N curve. The rule hypothesizes that fatigue damage is a result of the nucleation of microscopic voids, which cause crack initiation and crack propagation. The damage is described as a function of the number of damaged nuclei, the rate of damage propagation, and the accumulated loading cycles. The theory predicts the failure criterion as follows:

$$\sum_{1}^{i} \frac{n_i}{N_{fi,\max}\left(\frac{\sigma_{i,\max}}{\sigma_i}\right)^d} = 1 \tag{29}$$

where $\sigma_{i,\max}$ and $N_{fi,\max}$ denote the maximum loading stress level of applied loads and its fatigue life, respectively; d is a material parameter that is recommended as 4.8 for high strength steel and 5.8 for other materials.

Supposing that $\sigma_{i,\max} = \sigma_1$, Equation (29) can be rewritten as:

$$\sum D_i = \frac{n_1}{N_{f1}} + \frac{n_2}{N_{f2}}\frac{N_{f2}}{N_{f1}}\left(\frac{\sigma_2}{\sigma_1}\right)^d + \frac{n_3}{N_{f3}}\frac{N_{f3}}{N_{f1}}\left(\frac{\sigma_3}{\sigma_1}\right)^d + \frac{n_4}{N_{f4}}\frac{N_{f4}}{N_{f1}}\left(\frac{\sigma_4}{\sigma_1}\right)^d + \cdots = 1 \tag{30}$$

For each item in Equation (30), the damage variable is:

$$D_i = \frac{n_i}{N_{fi}} \times \frac{N_{fi}}{N_{f1}}\left(\frac{\sigma_i}{\sigma_1}\right)^d \tag{31}$$

In this model, the life fraction is amplified by a load effect coefficient with respect to applied loads, fatigue lives, and the exponent d. If the d value is identical to the material constant m in Equation (1), Equation (30) reduces to Equation (27), i.e., Miner rule.

2.2.3. Kwofie-Rahbar Rule (Kwofie's Model for Short)

Recently, Kwofie and Rahbar [31] proposed a fatigue driving stress concept to describe the damage accumulation process. The driving stress model is expressed by a function of expended life fraction, cyclic stress amplitude, and fatigue life. By using an equivalent driving stress approach similar to the equivalent damage rule [44], a cumulative damage model can be derived as follows:

$$\sum D_i = \frac{n_1}{N_{f1}} + \frac{n_2}{N_{f2}}\frac{\ln\left(N_{f2}\right)}{\ln\left(N_{f1}\right)} + \frac{n_3}{N_{f3}}\frac{\ln\left(N_{f3}\right)}{\ln\left(N_{f1}\right)} + \frac{n_4}{N_{f4}}\frac{\ln\left(N_{f4}\right)}{\ln\left(N_{f1}\right)} + \cdots = 1 \tag{32}$$

For each stage of loading amplitudes, the damage variable is defined as:

$$D_i = \frac{n_i}{N_{fi}} \times \frac{\ln\left(N_{fi}\right)}{\ln\left(N_{f1}\right)} \tag{33}$$

In the model, a load effect coefficient associated with the fatigue lives of the current load and the initial load is introduced to present the loading sequence effects. In particular, for constant amplitude loading, Equation (32) is reduced as the Miner rule.

3. Experiments and Discussions

In this section, the results from a series of two-stage and multi-stage experimental investigations are used to validate the proposed model. For the purpose of model comparison, three commonly used damage models, i.e., Miner rule, Corten's model, and Kwofie's model, are also employed to

compare with the proposed model on the predictive capability. According to the total amount of cumulative damage obtained by different models, the total fatigue life can be calculated by the following formula [45]:

$$N_{\text{pre}} = \frac{\sum_{i=1}^{k} n_i}{\sum_{i=1}^{k} D_i} \tag{34}$$

where N_{pre} denotes the predicted fatigue life. If the cumulative fatigue damage tends to unity (or the critical damage), then the predicted fatigue life should be close to the experimental result and the corresponding fatigue model becomes more effective.

3.1. Two-Stage Fatigue Loading

3.1.1. Results from Manson

The test material used here is the maraging 300 CVM steel [46] with the following mechanical properties: yield strength σ_s = 2098 MPa, ultimate strength σ_b = 2590 MPa, and fatigue limit σ_f = 662 MPa. The tests were conducted on a rotating-beam fatigue machine under rotating bending loading. Four sets of high-low load spectrums were chosen, i.e., 1111–833 MPa, 1372–1111 MPa, 1303–751 MPa, and 1095–751 MPa. The fatigue lives of the loading stress amplitudes are determined from the S-N curve data as listed in Table 1. The comparisons between the experimental and predicted results are summarized in Table 2 (N_{exp} is the experimental fatigue life) and represented in Figure 3.

Table 1. The loading stress amplitudes and their fatigue lives.

Stress Amplitude (MPa)	1372	1303	1111	1095	833	751
Fatigue Life (Cycles)	12,000	15,925	44,000	47,625	244,000	584,740

Table 2. Experimental data and models predictions for maraging 300 CVM steel.

Experimental Data			**Predicted Results Using Different Models**							
			Miner Rule		**Corten's Model**		**Kwofie's Model**		**Proposed Model**	
n_1	n_2	N_{exp}	N_{pre}	ΣD_i	N_{pre}	ΣD_i	N_{pre}	ΣD_i	N_{pre}	ΣD_i
High-low loading sequence: σ_1 = 1111 MPa, σ_2 = 833 MPa										
11,968	49,044	61,012	128,990	0.4730	126,630	0.4818	120,770	0.5052	93,120	0.6552
16,412	33,672	50,084	98,010	0.5110	96,870	0.5170	93,950	0.5331	72,190	0.6938
24,420	21,228	45,648	71,100	0.6420	70,680	0.6458	69,600	0.6559	54,940	0.8309
31,900	9028	40,928	53,710	0.7620	53,600	0.7636	53,300	0.7679	46,790	0.8747
High-low loading sequence: σ_1 = 1372 MPa, σ_2 = 1111 MPa										
960	24,684	25,644	40,010	0.6410	37,440	0.6850	35,690	0.7186	34,800	0.7370
948	40,832	41,780	41,490	1.0070	38,700	1.0797	36,800	1.1354	35,900	1.1638
4944	12,364	17,308	24,980	0.6930	24,210	0.7150	23,650	0.7319	17,760	0.9745
7404	8580	15,984	19,680	0.8120	19,320	0.8273	19,050	0.8390	14,280	1.1194
High-low loading sequence: σ_1 = 1303 MPa, σ_2 = 751 MPa										
971	367,810	368,781	534,470	0.6900	366,470	1.0063	399,030	0.9242	391,320	0.9424
1991	93,560	95,551	335,270	0.2850	261,430	0.3655	277,280	0.3446	218,350	0.4376
3790	45,610	49,400	156,330	0.3160	139,080	0.3552	143,190	0.3450	99,020	0.4989
7166	19,300	26,466	54,800	0.4830	52,970	0.4996	53,430	0.4953	37,260	0.7104
10,001	18,130	28,131	42,690	0.6590	41,700	0.6746	41,960	0.6705	26,280	1.0704
High-low loading sequence: σ_1 = 1095 MPa, σ_2 = 751 MPa										
3953	479,500	483,453	535,390	0.9030	398,590	1.2129	441,950	1.0939	400,310	1.2077
11,811	183,610	195,421	347,720	0.5620	287,090	0.6807	307,700	0.6351	195,710	0.9985
15,192	90,640	105,832	223,270	0.4740	198,710	0.5326	207,470	0.5101	136,190	0.7771
31,575	26,900	58,475	82,480	0.7090	80,500	0.7264	81,250	0.7197	59,810	0.9777

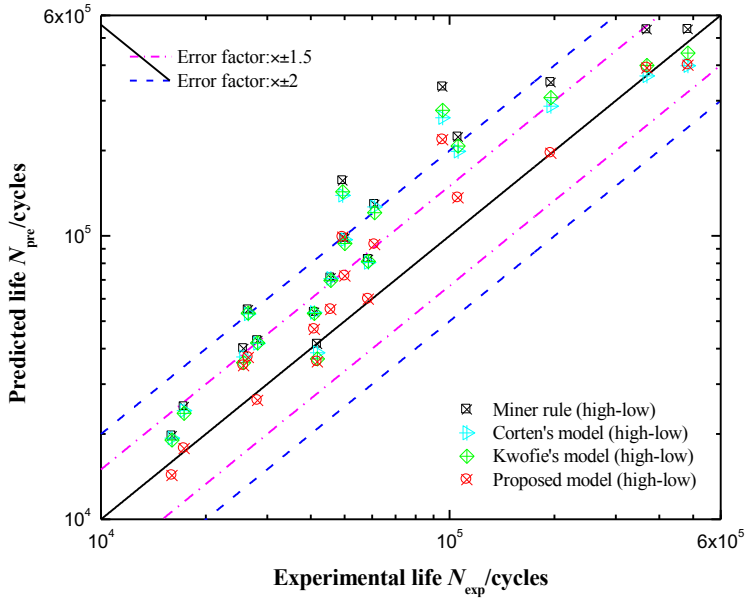

Figure 3. Comparison between the experimental lives and the predicted lives by Miner rule, Corten's model, Kwofie's model, and the proposed model for maraging 300 CVM steel.

3.1.2. Results from Pavlou

The tested material is the Al-2024-T42 aluminum alloy [9], which has been widely used in aerospace design. The polished specimens were subjected to complete reverse bending loading for both high-low and low-high loading sequences with several configurations of specified fatigue cycles. The loading stress ratio is set to be R = −1. The applied stress amplitudes are 200 MPa and 150 MPa, and the corresponding fatigue lives are 150,000 cycles and 430,000 cycles, respectively. Two sets of two-stage load spectrums are 200–150 MPa for high-low loading and 150–200 MPa for low-high loading, respectively. The comparisons of the observed and theoretical results are shown in Table 3 and illustrated in Figure 4.

Table 3. Experimental data and models predictions for Al-2024-T42 aluminum alloy.

Experimental Data			Predicted Results Using Different Models							
			Miner Rule		Corten's Model		Kwofie's Model		Proposed Model	
n_1	n_2	N_{exp}	N_{pre}	ΣD_i	N_{pre}	ΣD_i	N_{pre}	ΣD_i	N_{pre}	ΣD_i
High-low loading sequence: σ_1 = 200 MPa, σ_2 = 150 MPa										
30,000	259,100	289,100	360,020	0.8030	549,620	0.5260	337,730	0.8560	284,830	1.0150
	233,400	263,400	354,510	0.7430	534,280	0.4930	333,000	0.7910	282,010	0.9340
	193,500	223,500	343,850	0.6500	504,510	0.4430	323,910	0.6900	276,270	0.8090
60,000	90,300	150,300	246,390	0.6100	292,410	0.5140	238,950	0.6290	196,730	0.7640
	98,250	158,250	251,590	0.6290	302,000	0.5240	243,840	0.6490	198,810	0.7960
	114,600	174,600	261,770	0.6670	320,960	0.5440	253,040	0.6900	202,550	0.8620
90,000	86,000	176,000	220,000	0.8000	248,590	0.7080	215,160	0.8180	171,880	1.0240
	42,300	132,300	189,540	0.6980	202,600	0.6530	187,130	0.7070	163,540	0.8090
	99,800	189,800	228,130	0.8320	261,790	0.7250	222,510	0.8530	173,810	1.0920
Low-high loading sequence: σ_1 = 150 MPa, σ_2 = 200 MPa										
86,000	138,000	224,000	200,000	1.1200	217,900	1.0280	214,350	1.0450	254,550	0.8800
	147,000	233,000	197,460	1.1800	214,150	1.0880	211,820	1.1000	251,890	0.9250
	148,500	234,500	197,060	1.1900	213,570	1.0980	211,260	1.1100	251,610	0.9320
172,000	138,000	310,000	234,850	1.3200	272,890	1.1360	249,000	1.2450	332,980	0.9310
	139,500	311,500	234,210	1.3300	271,820	1.1460	248,210	1.2550	332,440	0.9370
	123,000	295,000	241,800	1.2200	284,750	1.0360	255,850	1.1530	337,920	0.8730
258,000	89,000	347,000	290,860	1.1930	378,000	0.9180	303,060	1.1450	394,320	0.8800
	81,000	339,000	297,370	1.1400	392,360	0.8640	309,310	1.0960	396,490	0.8550
	75,000	333,000	302,730	1.1000	404,130	0.8240	314,450	1.0590	398,330	0.8360

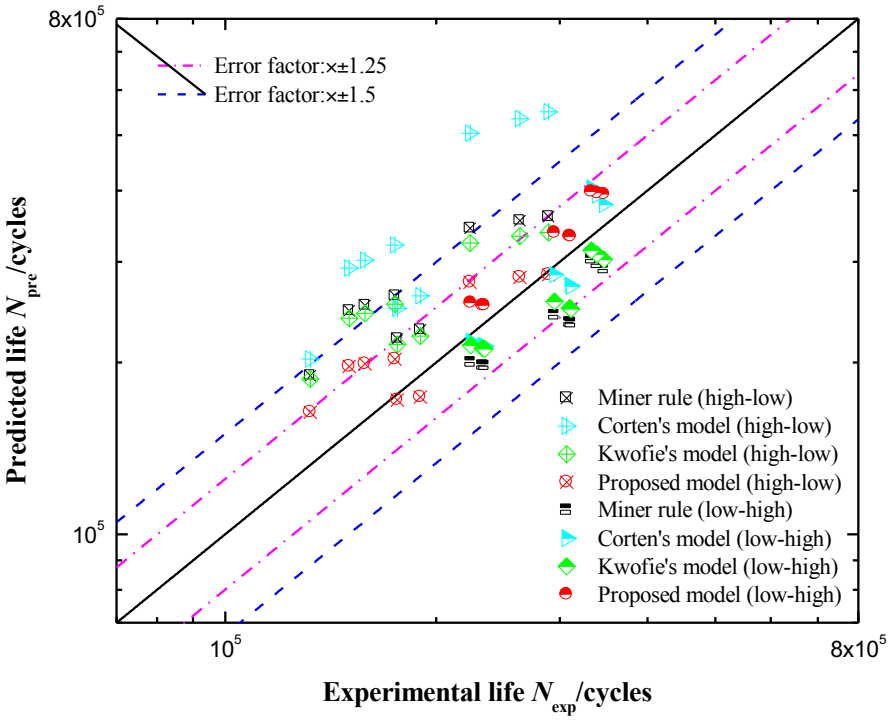

Figure 4. Comparison between the experimental lives and the predicted lives by Miner rule, Corten's model, Kwofie's model, and the proposed model for Al-2024-T42 aluminum alloy.

3.1.3. Results from Dattoma

The material tested is a hardened and tempered 30NiCrMoV12 steel [47,48], which is mainly used for railway axle applications. The mechanical properties of the material are listed as: Young's modulus E = 201.4 GPa, fatigue limit σ_f = 391 MPa, yield strength σ_s = 755 MPa, and ultimate strength σ_b = 1035 MPa. The tests were carried out on a servo-hydraulic MTS810 testing machine under oscillating tensile-compression loading in stress-controlled mode with R = −1. Five loading stress amplitudes are chosen, i.e., 485 MPa, 465 MPa, 450 MPa, 420 MPa, and 400 MPa, and their fatigue lives, determined from the S-N curve at 50% of probability of failure, are 54,998 cycles, 68,053 cycles, 80,330 cycles, 113,876 cycles, and 145,749 cycles, respectively. Three sets of two-stage high-low load spectrums are 485–400 MPa, 465–420 MPa, and 450–420 MPa, respectively. Three sets of two-stage low-high load spectrums are 400–485 MPa, 420–465 MPa, and 420–450 MPa, respectively. The comparisons between the observed results and models predictions are given in Table 4 and depicted in Figure 5.

To clearly show the predicted results, the scatter band is used to assess the predictive capability, as shown in Figures 2–4. It is observed that the proposed model shows a good agreement between the experimental and theoretical results. From Tables 2–4, the cumulative damage calculated by the proposed model is found to be closer to unity than that of other models, and resulting in more accurate fatigue lives.

Among three typical damage models, the Miner rule has the simplest form that the segmental damage for each loading stress level is defined as a life fraction, but it fails to account for the effects of loading histories as a result of large prediction errors. The Corten's model improves the Miner rule by modifying the S-N curve slope to consider load interaction effects, while the exploration of the predictions still shows a large deviation. This might be attributed to that the chosen value of the exponent d in Equation (31) is taken as an empirical constant, which is in reality independent of the loading histories. The Kwofie's model is designed to consider the loading sequence effects, yet the predicted results by the model are slightly better than the counterparts from the Miner rule. It could

be explained by the fact that the load effect coefficient in Equation (33) only relates to the initial and current fatigue lives, regardless of previous loading cycles on damage accumulation.

Table 4. Experimental data and models predictions for 30NiCrMoV12 steel.

Experimental Data			Predicted Results Using Different Models							
			Miner Rule		Corten's Model		Kwofie's Model		Proposed Model	
n_1	n_2	N_{exp}	N_{pre}	ΣD_i	N_{pre}	ΣD_i	N_{pre}	ΣD_i	N_{pre}	ΣD_i
High-low loading sequence: σ_1 = 485 MPa, σ_2 = 400 MPa										
13,749	51,304	65,053	108,060	0.6020	117,190	0.5551	102,700	0.6334	87,310	0.7451
27,499	45,765	73,264	90,000	0.8140	94,880	0.7722	87,010	0.8420	68,090	1.0760
41,249	16,032	57,281	66,610	0.8600	67,760	0.8453	65,860	0.8698	57,390	0.9981
High-low loading sequence: σ_1 = 465 MPa, σ_2 = 420 MPa										
17,013	66,845	83,858	100,190	0.8370	105,570	0.7943	97,040	0.8642	88,000	0.9529
34,027	30,405	64,432	84,010	0.7670	86,190	0.7476	82,670	0.7794	74,240	0.8679
51,040	38,262	89,302	82,230	1.0860	84,120	1.0616	81,070	1.1015	70,520	1.2664
High-low loading sequence: σ_1 = 450 MPa, σ_2 = 420 MPa										
20,082	79,372	99,454	105,020	0.9470	109,030	0.9122	102,690	0.9685	95,860	1.0375
40,165	24,711	64,876	90,480	0.7170	91,870	0.7062	89,640	0.7237	84,300	0.7696
60,248	15,943	76,191	85,610	0.8900	86,290	0.8830	85,200	0.8943	81,290	0.9373
Low-high loading sequence: σ_1 = 400 MPa, σ_2 = 485 MPa										
36,440	53,348	89,788	73,600	1.2200	75,660	1.1867	78,730	1.1405	95,550	0.9397
72,870	45,373	118,243	89,240	1.3250	93,960	1.2584	94,040	1.2574	124,490	0.9498
109,310	46,693	156,003	97,560	1.5990	104,060	1.4991	102,000	1.5294	138,500	1.1264
Low-high loading sequence: σ_1 = 420 MPa, σ_2 = 465 MPa										
28,469	58,594	87,063	78,360	1.1110	79,670	1.0928	81,150	1.0729	89,840	0.9691
56,938	56,416	113,354	85,290	1.3290	87,690	1.2926	87,710	1.2923	102,890	1.1017
85,407	48,998	134,405	91,430	1.4700	94,960	1.4154	93,450	1.4382	110,300	1.2185
Low-high loading sequence: σ_1 = 420 MPa, σ_2 = 450 MPa										
28,469	70,530	98,999	87,770	1.1280	88,750	1.1155	89,860	1.1017	96,390	1.0271
56,938	39,362	96,300	97,270	0.9900	99,790	0.9650	98,740	0.9753	107,680	0.8943
85,407	10,523	95,930	108,890	0.8810	113,720	0.8436	109,370	0.8771	113,140	0.8479

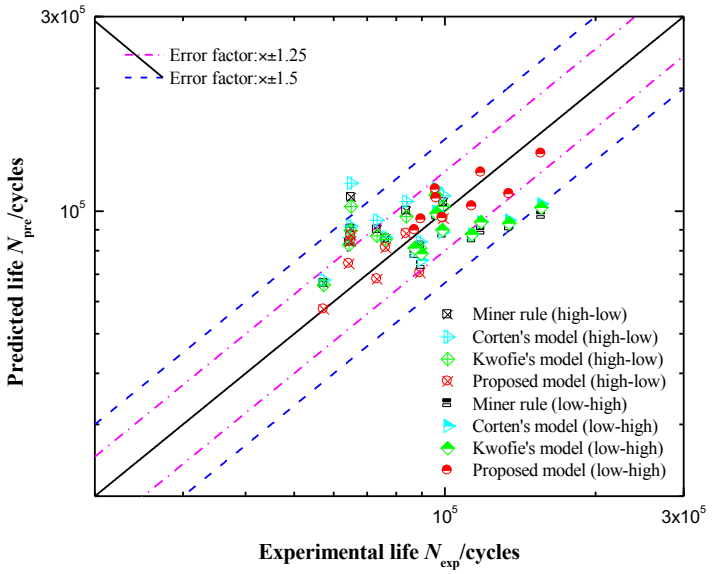

Figure 5. Comparison between the experimental lives and the predicted lives by Miner rule, Corten's model, Kwofie's model, and the proposed model for 30NiCrMoV12 steel.

Through comparison with the above-mentioned models, the proposed model in the form of Equation (25) is closely linked to the expended life fractions and fatigue lives of previous loads. The model takes more fatigue loading history information into account and thus leads to relatively small prediction errors. It should be noted that the model follows a simple linear trend in accumulating fatigue damage and also accounts for load-level dependence and loading sequence effects. Consequently, the cumulative damage model presented here is expected to be reasonable and it should be easy to calculate damage and fatigue life using the conventional S-N curve data.

3.2. Multi-Stage Fatigue Loading

In order to further demonstrate the effectiveness of the proposed model, results from the multi-stage fatigue loading test data available in the literature are used. The tested material is 41Cr4 [45] with the following mechanical properties: ultimate strength σ_b = 850~900 MPa and fatigue limit σ_f = 173.5 MPa. Two sets of cumulative fatigue damage (CFD) tests, i.e., CFD1 test and CFD2 test, were performed under cyclic bending loading with R = −1. To check the capability of the predicted fatigue lives, the relative forecast error δ is employed and defined as follows:

$$\delta(\%) = \left| \frac{N_{pre} - N_{exp}}{N_{exp}} \right| \times 100 \tag{35}$$

3.2.1. Results from CFD1 Test

In the test, the cylindrical specimen was subjected to eight-stage high-low fatigue loading with six stress levels above the fatigue limit. The experimental fatigue life at fracture is $N_{exp} = 2.00 \times 10^6$ cycles. The loading test parameters and the predicted damage are listed in Table 5. A comparison of models prediction performances is shown in Table 6.

Table 5. Experimental data and the predicted damage for CFD1 test.

Stress Level	Stress Amplitude, σ_i (MPa)	n_i (Cycles)	N_{fi} (Cycles)	Segmental Damage Caused by Each Stress Level			
				Miner Rule	Corten's Model	Kwofie's Model	Proposed Model
1	505	4	9.00×10^3	0.0004	0.0004	0.0004	0.0004
2	475	32	1.16×10^4	0.0028	0.0025	0.0029	0.0028
3	423	560	2.10×10^4	0.0267	0.0223	0.0292	0.0268
4	362	5440	4.70×10^4	0.1158	0.0877	0.1368	0.1206
5	287	40,000	1.55×10^5	0.2580	0.1676	0.3387	0.3458
6	212	184,000	8.70×10^5	0.2110	0.1328	0.3169	0.6645
7	137	560,000	∞	0	0	0	0
8	63	1,210,000	∞	0	0	0	0

Table 6. Prediction performances of Miner rule, Corten's model, Kwofie's model, and the proposed model for CFD1 test.

Prediction Performance	Experimetal Result	Miner Rule	Corten's Model	Kwofie's Model	Proposed Model
$\sum_{i=1}^{8} D_i$	1	0.6147	0.4133	0.8249	1.1609
Predicted fatigue life N_{pre} (cycles)	2.00×10^6	3.25×10^6	4.84×10^6	2.42×10^6	1.72×10^6
Relative forecast error δ (%)	—	62.50	142.00	21.00	14.00

3.2.2. Results from CFD2 Test

The test was carried out under eight-stage high-low fatigue loading with five stress levels above the fatigue limit. The experimental fatigue life is $N_{exp} = 2.20 \times 10^7$ cycles. The models predictions and the corresponding prediction performances are shown in Tables 7 and 8, respectively.

Table 7. Experimental data and the predicted damage for CFD2 test.

Stress Level	Stress Amplitude, σ_i (MPa)	n_i (cycles)	N_{fi} (cycles)	Segmental Damage Caused by Each Stress Level			
				Miner Rule	Corten's Model	Kwofie's Model	Proposed Model
1	350	44	5.60×10^4	0.0008	0.0008	0.0008	0.0008
2	332	352	7.40×10^4	0.0047	0.0046	0.0048	0.0047
3	298	6160	1.30×10^5	0.0475	0.0434	0.0512	0.0477
4	254	59,840	2.80×10^5	0.2140	0.1667	0.2455	0.2290
5	201	440,000	1.25×10^6	0.3520	0.3149	0.4520	0.6468
6	149	2,024,000	∞	0	0	0	0
7	96	6,160,000	∞	0	0	0	0
8	44	13,310,000	∞	0	0	0	0

Table 8. Prediction performances of Miner rule, Corten's model, Kwofie's model, and the proposed model for CFD2 test.

Prediction Performance	Experimetal Result	Miner Rule	Corten's Model	Kwofie's Model	Proposed Model
$\sum_{i=1}^{8} D_i$	1	0.6190	0.6631	0.7543	0.9290
Predicted fatigue life N_{pre} (cycles)	2.20×10^7	3.55×10^7	3.32×10^7	2.92×10^7	2.37×10^7
Relative forecast error δ (%)	—	61.36	50.91	32.73	7.73

According to Tables 6 and 8, it can be seen that the proposed model predicts the cumulative damage closer to unity and more accurate fatigue lives than three typical models. Tables 5 and 7 list the segmental damage predicted by different models. It should be pointed out that the segmental damage caused by the stress levels below the fatigue limit is negligible.

From the above-mentioned two cases, the predictions using the Miner rule show a large deviation with the experimental data, due to the lack of loading history effects. The Corten's model and the Kwofie's model are also found to predict large deviations, because their load effect coefficients only relate to limited fatigue loadings. This may not be sufficient to characterize the complex behaviors of loading histories, especially for multi-stage variable loadings. It should be anticipated that the proposed damage model shows a high sensitivity to the details of previous fatigue loadings with more loading histories for consideration and thus predicts better results.

Furthermore, some common characteristics and fundamental properties of the chosen fatigue models can be extracted as follows:

(1) In the models, the damage variable can be characterized by a general form available for different loading amplitudes. Fatigue damage is accumulated by adding up the segmental damage caused by each loading stress level. These models are essentially the LDRs, and this makes it convenient to calculate damage and fatigue life, compared with various non-linear theories.

(2) Miner rule defines the damage variable as a life fraction regardless of loading histories accountability, while three typical damage models improve this basic rule by multiplying a load effect coefficient, which tends to consider previous fatigue loadings on damage accumulation.

(3) For constant amplitude loading, the proposed model, Corten's model, and Kwofie's model will degenerate to the Miner rule. It can be concluded that the Miner rule forms a particular basis for these linear extensions and should be sufficient to assess fatigue damage under constant amplitude loading because loading history effects can be ignored under such loading condition.

The findings obtained in this study are based on the S-N curve approach and should be restricted to the applicable range of high-cycle fatigue regime. The proposed model is calibrated by the uniaxial fatigue experimental data, and may be extended to the field of multiaxial fatigue criterion. The model improves some of the shortcomings of the Miner rule, but the void response for low amplitude loads below the fatigue limit still remains [49]. The cumulative damage formula of Equation (26)

can also be improved by adjusting the critical failure criterion (conventionally, D_f = 1), depending on the material properties, external loads, and safety factor, for increased prediction accuracy and fatigue resistant design. The fatigue modeling presented here pertains to a deterministic methodology, whereas the fatigue process is stochastic in nature with various uncertainties [50–52], such as load variation, model parameters, and statistical errors. Therefore, further insights into these uncertainties on fatigue are still in demand.

4. Conclusions

In this paper, the S-N curve approach is used to deal with the development of variable amplitude fatigue damage. From the present comparisons between the published experimental data and theoretical results, some conclusions can be drawn as follows:

(1) A phenomenological cumulative damage rule is proposed by incorporating a dynamic residual S-N curve and material memory concept to describe damage accumulation behavior. The model follows a linear trend in accumulating damage and also takes the load-level dependence and loading sequences into account. It predicts the damage and fatigue life with a small amount of data necessary from the conventional S-N curve.

(2) The proposed model is calibrated and verified by a series of non-uniform fatigue loading protocols. Comparing with the commonly used damage rules, the model predicts the cumulative damage closer to unity and more accurate fatigue lives. The present damage formula shows a high sensitivity to the details of previous fatigue loadings with more loading histories for consideration.

(3) Several common characteristics and fundamental properties of the chosen fatigue models are briefly discussed. Miner rule is improved by multiplying a load effect coefficient with respect to previous fatigue loadings for three typical damage models. In particular, the Miner rule is also found to form a general basis for these linear extensions under constant amplitude loadings.

Author Contributions: Formal analysis, J.Z.; Funding acquisition, Y.-F.L.; Methodology, Z.P.; Supervision, H.-Z.H.; Validation, Y.-F.L.; Writing—original draft, Z.P.; Writing—review & editing, H.-Z.H.

Acknowledgments: This study was sponsored by the National Natural Science Foundation of China under Grant No. 51775090.

Conflicts of Interest: The authors declare no conflict of interest.

References

1. Chaboche, J.L. Continuous damage mechanics—A tool to describe phenomena before crack initiation. *Nucl. Eng. Des.* **1981**, *64*, 233–247. [CrossRef]
2. Lubarda, V.A.; Krajcinovic, D. Damage tensors and the crack density distribution. *Int. J. Solids Struct.* **1993**, *30*, 2859–2877. [CrossRef]
3. Voyiadjis, G.Z.; Kattan, P.I. A comparative study of damage variables in continuum damage mechanics. *Int. J. Damage Mech.* **2009**, *18*, 315–340. [CrossRef]
4. Rejovitzky, E.; Altus, E. On single damage variable models for fatigue. *Int. J. Damage Mech.* **2013**, *22*, 268–284. [CrossRef]
5. Peng, Z.; Huang, H.Z.; Wang, H.K.; Zhu, S.P.; Lv, Z. A new approach to the investigation of load interaction effects and its application in residual fatigue life prediction. *Int. J. Damage Mech.* **2016**, *25*, 672–690. [CrossRef]
6. Hu, D.; Wang, R.; Fan, J.; Shen, X. Probabilistic damage tolerance analysis on turbine disk through experimental data. *Eng. Fract. Mech.* **2012**, *87*, 73–82. [CrossRef]
7. Tanaka, K.; Mura, T. A dislocation model for fatigue crack initiation. *J. Appl. Mech.* **1981**, *48*, 97–103. [CrossRef]
8. Fedelich, B. A stochastic theory for the problem of multiple surface crack coalescence. *Int. J. Fract.* **1998**, *91*, 23–45. [CrossRef]
9. Pavlou, D.G. A phenomenological fatigue damage accumulation rule based on hardness increasing, for the 2024-T42 aluminum. *Eng. Struct.* **2002**, *24*, 1363–1368. [CrossRef]

10. Naderi, M.; Khonsari, M.M. A thermodynamic approach to fatigue damage accumulation under variable loading. *Mater. Sci. Eng. A-Struct.* **2010**, *527*, 6133–6139. [CrossRef]
11. Li, Y.F.; Lv, Z.; Cai, W.; Zhu, S.P.; Huang, H.Z. Fatigue life analysis of turbine disks based on load spectra of aero-engines. *Int. J. Turbo Jet-Eng.* **2016**, *33*, 27–33. [CrossRef]
12. Yu, L.; Chen, H.; Zhou, J.; Yin, H.; Huang, H.Z. Fatigue life prediction of low pressure turbine shaft of turbojet engine. *Int. J. Turbo Jet-Eng.* **2017**, *34*, 149–154. [CrossRef]
13. Hou, S.Q.; Cai, X.J.; Xu, J.Q. A life evaluation formula for high cycle fatigue under uniaxial and multiaxial loadings with mean stresses. *Int. J. Mech. Sci.* **2015**, *93*, 229–239. [CrossRef]
14. Zhang, W.; Zhou, Z.; Zhang, B.; Zhao, S. A phenomenological fatigue life prediction model of glass fiber reinforced polymer composites. *Mater. Des.* **2015**, *66*, 77–81. [CrossRef]
15. Fatemi, A.; Yang, L. Cumulative fatigue damage and life prediction theories: A survey of the state of the art for homogeneous materials. *Int. J. Fatigue* **1998**, *20*, 9–34. [CrossRef]
16. Schijve, J. *Fatigue of Structures and Materials*; Springer Science & Business Media: Berlin, Germany, 2001.
17. Miner, M.A. Cumulative damage in fatigue. *J. Appl. Mech.* **1945**, *12*, 159–164.
18. Manson, S.S.; Halford, G.R. Practical implementation of the double linear damage rule and damage curve approach for treating cumulative fatigue damage. *Int. J. Fract.* **1981**, *17*, 169–192. [CrossRef]
19. Liu, Y.; Mahadevan, S. Stochastic fatigue damage modeling under variable amplitude loading. *Int. J. Fatigue* **2007**, *29*, 1149–1161. [CrossRef]
20. Mi, J.; Li, Y.F.; Peng, W.; Huang, H.Z. Reliability analysis of complex multi-state system with common cause failure based on evidential networks. *Reliab. Eng. Syst. Saf.* **2018**, *174*, 71–81. [CrossRef]
21. Li, X.Y.; Huang, H.Z.; Li, Y.F.; Zio, E. Reliability assessment of multi-state phased mission system with non-repairable multi-state components. *Appl. Math. Model.* **2018**, *61*, 181–199. [CrossRef]
22. Huang, H.Z.; Huang, C.G.; Peng, Z.; Li, Y.F.; Yin, H. Fatigue life prediction of fan blade using nominal stress method and cumulative fatigue damage theory. *Int. J. Turbo Jet Eng.* **2017**. [CrossRef]
23. Lv, Z.; Huang, H.Z.; Zhu, S.P.; Gao, H.; Zuo, F. A modified nonlinear fatigue damage accumulation model. *Int. J. Damage Mech.* **2015**, *24*, 168–181. [CrossRef]
24. Zuo, F.J.; Huang, H.Z.; Zhu, S.P.; Lv, Z.; Gao, H. Fatigue life prediction under variable amplitude loading using a non-linear damage accumulation model. *Int. J. Damage Mech.* **2015**, *24*, 767–784. [CrossRef]
25. Corten, H.T.; Dolan, T.J. Cumulative fatigue damage. In Proceedings of the International Conference on Fatigue of Metals, London, UK, 10–14 September 1956.
26. Freudenthal, A.M.; Heller, R.A. On stress interaction in fatigue and a cumulative damage rule. *J. Aerosp. Sci.* **1959**, *26*, 431–442. [CrossRef]
27. Subramanyan, S. A cumulative damage rule based on the knee point of the S-N curve. *J. Eng. Mater. Technol.* **1976**, *98*, 316–321. [CrossRef]
28. Hashin, Z.; Rotem, A. A cumulative damage theory of fatigue failure. *Mater. Sci. Eng.* **1978**, *34*, 147–160. [CrossRef]
29. Leipholz, H.H.E. On the modified S-N curve for metal fatigue prediction and its experimental verification. *Eng. Fract. Mech.* **1986**, *23*, 495–505. [CrossRef]
30. EI Aghoury, I.; Galal, K. A fatigue stress-life damage accumulation model for variable amplitude fatigue loading based on virtual target life. *Eng. Struct.* **2013**, *52*, 621–628. [CrossRef]
31. Kwofie, S.; Rahbar, N. A fatigue driving stress approach to damage and life prediction under variable amplitude loading. *Int. J. Damage Mech.* **2013**, *22*, 393–404. [CrossRef]
32. Peng, Z.; Huang, H.Z.; Zhu, S.P.; Gao, H.; Lv, Z. A fatigue driving energy approach to high—cycle fatigue life estimation under variable amplitude loading. *Fatigue Fract. Eng. Mater.* **2016**, *39*, 180–193. [CrossRef]
33. Mesmacque, G.; Garcia, S.; Amrouche, A.; Rubio-Gonzalez, C. Sequential law in multiaxial fatigue, a new damage indicator. *Int. J. Fatigue* **2005**, *27*, 461–467. [CrossRef]
34. Aïd, A.; Amrouche, A.; Bouiadjra, B.B.; Benguediab, M.; Mesmacque, G. Fatigue life prediction under variable loading based on a new damage model. *Mater. Des.* **2011**, *32*, 183–191. [CrossRef]
35. Aid, A.; Bendouba, M.; Aminallah, L.; Amrouche, A.; Benseddiq, N.; Benguediab, M. An equivalent stress process for fatigue life estimation under multiaxial loadings based on a new non linear damage model. *Mater. Sci. Eng. A Struct.* **2012**, *538*, 20–27. [CrossRef]

36. Djebli, A.; Aid, A.; Bendouba, M.; Amrouche, A.; Benguediab, M.; Benseddiq, N. A non-linear energy model of fatigue damage accumulation and its verification for Al-2024 aluminum alloy. *Int. J. Nonlinear Mech.* **2013**, *51*, 145–151. [CrossRef]
37. Benkabouche, S.; Guechichi, H.; Amrouche, A.; Benkhettab, M. A modified nonlinear fatigue damage accumulation model under multiaxial variable amplitude loading. *Int. J. Mech. Sci.* **2015**, *100*, 180–194. [CrossRef]
38. Rege, K.; Pavlou, D.G. A one-parameter nonlinear fatigue damage accumulation model. *Int. J. Fatigue* **2017**, *98*, 234–246. [CrossRef]
39. Pavlou, D.G. The theory of the s-n fatigue damage envelope: Generalization of linear, double-linear, and non-linear fatigue damage models. *Int. J. Fatigue* **2018**, *110*, 204–214. [CrossRef]
40. Böhm, E.; Kurek, M.; Junak, G.; Cieśla, M.; Łagoda, T. Accumulation of fatigue damage using memory of the material. *Procedia Mater. Sci.* **2014**, *3*, 2–7. [CrossRef]
41. Basquin, O.H. *The Exponential Law of Endurance Tests*; American Society for Testing and Materials: Phildelphia, PA, USA, 1910.
42. Böhm, E.; Kurek, M.; Łagoda, T. Accumulation of fatigue damages for block-type loads with use of material memory function. In *Solid State Phenomena*; Trans Tech Publications: Zürich, Switzerland, 2015; Volume 224, pp. 39–44.
43. Ebbinghaus, H. *Memory*; Columbia University, Teachers College: New York, NY, USA, 1913.
44. Richart, F.E.; Newmark, N.M. *A Hypothesis for the Determination of Cumulative Damage in Fatigue*; American Society for Testing and Materials: Phildelphia, PA, USA, 1948.
45. Li, M.; Otto, B. *Anti-Fatigue Design for Structural Components*; China Machine Press: Beijing, China, 1987.
46. Manson, S.S.; Freche, J.C.; Ensign, C.R. Application of a double linear damage rule to cumulative fatigue. In *Fatigue Crack Propagation*; ASTM STP 415; American Society for Testing and Materials: Philadelphia, PA, USA, 1967.
47. Dattoma, V.; Giancane, S.; Nobile, R.; Panella, F.W. Fatigue life prediction under variable loading based on a new non-linear continuum damage mechanics model. *Int. J. Fatigue* **2006**, *28*, 89–95. [CrossRef]
48. Giancane, S.; Nobile, R.; Panella, F.W.; Dattoma, V. Fatigue life prediction of notched components based on a new nonlinear continuum damage mechanics model. *Procedia Eng.* **2010**, *2*, 1317–1325. [CrossRef]
49. Zhou, J.; Huang, H.Z.; Peng, Z. Fatigue life prediction of turbine blades based on modified equivalent strain model. *J. Mech. Sci. Technol.* **2017**, *31*, 4203–4213. [CrossRef]
50. Hu, D.; Ma, Q.; Shang, L.; Gao, Y.; Wang, R. Creep-fatigue behavior of turbine disc of superalloy GH720Li at 650 C and probabilistic creep-fatigue modeling. *Mater. Sci. Eng. A-Struct.* **2016**, *670*, 17–25. [CrossRef]
51. Zheng, B.; Huang, H.Z.; Guo, W.; Li, Y.F.; Mi, J. Fault diagnosis method based on supervised particle swarm optimization classification algorithm. *Intell. Data Anal.* **2018**, *22*, 191–210. [CrossRef]
52. Li, X.Y.; Huang, H.Z.; Li, Y.F. Reliability analysis of phased mission system with non-exponential and partially repairable components. *Reliab. Eng. Syst. Saf.* **2018**, *175*, 119–127. [CrossRef]